WAPD-T-3138

CONF-970490--2

The Effect of Potential Upon the High-Temperature Fatigue Crack Growth Response of Low-Alloy Steels, Part I: Crack Growth Results

L. A. James and W. C. Moshier

U.S. Department of Energy Contract DE-AC11-93PN38195

Paper Proposed for Publication in Corrosion Science

BETTIS ATOMIC POWER LABORATORY PITTSBURGH, PENNSYLVANIA 15122-0079

Operated for the U.S. Department of Energy
by WESTINGHOUSE ELECTRIC CORPORATION

The Effect of Potential Upon the High-Temperature Fatigue Crack Growth Response of Low-Alloy Steels, Part I: Crack Growth Results

L. A. James and W. C. Moshier
Bettis Atomic Power Laboratory
Westinghouse Electric Corporation
West Mifflin, PA 15122-0079

ABSTRACT

Corrosion-fatigue crack propagation experiments were conducted on several low-alloy steels in elevated temperature aqueous environments, and experimental parameters included temperature, sulfur content of the steel, applied potential level, and dissolved hydrogen (and in one case, dissolved oxygen) concentration in the water. Specimen potentials were controlled potentiostatically, and the observation (or non-observation) of accelerated fatigue crack growth rates was a complex function of the above parameters. Electrochemical results and the postulated explanation for the complex behavior are given in Part II.

DISCLAIMER

INTRODUCTION

The subject of environmentally-assisted cracking (EAC) of low-alloy steels in high-temperature aqueous environments has attracted a great deal of research interest since the pioneering work of Kondo et al.[1,2] showed that fatigue crack propagation (FCP) rates could be one to two orders of magnitude higher in the aqueous environment than in air under the equivalent loading conditions. Scores of research papers on EAC in low-alloy steels have appeared in the literature in the intervening years, and the basic cause-and-effect relationships are now relatively well understood; e.g., review articles on the phenomenon may be found in References 3-5. EAC develops when the crack-tip concentration of H_2S reaches a "critical" value of about 5 ± 2 ppm[6]. The crack-tip sulfide concentration at any point in time is the net balance between the competing processes of sulfide supply and sulfide loss. In lieu of water-borne sulfur contamination, the only source of sulfur supply to the crack tip is from within the steel itself. Metallurgical sulfide inclusions (e.g., MnS, FeS, etc.) within the steel are intersected by the growing crack, and are readily soluble in the crack-tip environment.[7,8] Sulfides may be removed from the crack tip by any one, or more, of four different mass-transport processes: 1) diffusion due to a sulfide concentration gradient from the crack tip to the crack mouth,[9-11] 2) ion migration due to an electrochemical corrosion potential (ECP) gradient from the crack tip to the crack mouth,[9,10] 3) fatigue "pumping" or advection due to the cyclic motion of the crack flanks,[12,13] and 4) convective mass transport induced within the crack enclave by an external (to the crack) stream flow. [14,15] Not all of these mass-transport processes play a significant role in every case of corrosion-FCP of low-alloy steels in high-temperature aqueous environments. For example, the second process, ion migration, is probably more of a factor in oxygenated Boiling Water Reactor (BWR) environments than in low-oxygen Pressurized Water Reactor (PWR) environments, because in BWR environments a significant ECP gradient can exist between the crack mouth and the crack tip.[16] The gradient in ECP from the crack mouth to the tip is much lower in PWR environments.[16] The third mass-transport process, fatigue "pumping", is likely to be a factor only at relatively high cyclic frequencies, and the fourth process, convective mass transport, would not be an important consideration under quasi-stagnant flow conditions. The present work will explore the effects of ion migration by use of a potentiostatic control technique.

EXPERIMENTAL PROCEDURES

This portion of the study (Part 1) will deal primarily with the crack propagation response, while Part 2[17] will deal primarily with the electrochemical response. Therefore the present section on experimental procedures will deal mainly with those related to the FCP testing.

Four steels of differing sulfur content were employed in this study, and they are designated as steels "A" through "D". The steels are identified, along with their chemical compositions and room temperature tensile properties in Tables I and II, respectively. Steel "A" was a low-sulfur and low-residual element forging that has been called "superclean".[18] Steel "B" was a medium-sulfur ASTM A508-2 (UNS K12766) forging, and Steel "C" was a medium-sulfur ASTM A508-4 (UNS K22375) forging. Steel "D" was a high-sulfur ASTM A302-B (UNS K12022) plate which has exhibited EAC in low-oxygen water in several previous studies.[14,15,19] The Charpy impact toughness of Steels "A", "C", and "D" was presented in Reference 18, and the elevated temperature tensile and strain-hardening behavior of Steel "D" was given in Reference 20.

Two FCP specimen designs were employed in this study: a 1T-CT compact tension design (H/W = 0.6, W = 50.8 mm), and a 1T-WOL design (wedge-opening-load, H/W = 0.486, W = 64.77 mm). Stress-intensity factor (K) solutions for both designs are given by Saxena and Hudak.[21] Crack lengths were inferred from compliance measurements made using an *in-situ* transducer and the compliance relationships of Saxena and Hudak.[21] The experiments on Steel "A" employed the 1T-WOL design, while the other experiments employed the 1T-CT design. Cyclic loadings were applied using a feedback-controlled servo-hydraulic loading system. A "positive sawtooth" loading waveform (85% load rise-time, 15% load fall-time) was used for all of the experiments.

Deaerated water with a low-level of dissolved oxygen (DO_2 < 10 ppb) was utilized; Experiment 3 was an exception because DO_2 was a parameter in that experiment. Room temperature pH was about 10.2, and the calculated* pH at the two test temperatures of 149°C and 243°C was 7.7 and 6.8, respectively. Room temperature conductivity was generally about 48 $\pm$ 5 μS/cm. The level of dissolved hydrogen (DH_2) was a test parameter, and "low-hydrogen" conditions were generally DH_2 < 1 cc H_2/kg H_2O (<8.2 ppb), while "high-

* Calculated using MULTEQ (® Electric Power Research Institute)

hydrogen" conditions were generally in the range 30 < DH_2 < 55 cc H_2/kg H_2O (2.5 to 4.5 ppm). The experiments were conducted in an autoclave of approximately 19 liters volume, and the refreshment rate was approximately 50 cc/minute. Hence, on the average, about 6.3 hours would be required for one volume change of water; i.e.; quiescent flow conditions.

The electrochemical test methodology will be described in greater detail in Part 2.[17] An external Ag/AgCl/0.1 N KCl reference electrode was employed to measure the specimen potential. The measurements were converted to Standard Hydrogen Electrode (SHE) conditions using the relationship of Macdonald et al.[22]. Potentials were applied to the FCP specimens using a Gamry® PC3 potentiostat with CMS 100 software (see Part 2[17] for greater detail). The lower levels of DH_2 were measured using a Model 3600 hydrogen Orbisphere® with a 2956A membrane capable of monitoring DH_2 gas concentrations between 0.03-75 ppb. The higher levels of DH_2 were measured in most cases by extracting test solution from the chemistry tank using a syringe and injecting it into a thermal conductivity cell hydrogen analyzer, while an Orbisphere (fitted with a thicker membrane) was employed for the remainder of the measurements.

Nine experiments were conducted in this study, and the experiments conducted under low-DH_2 conditions will be discussed first, followed by those under high-DH_2 conditions.

RESULTS AND DISCUSSION

Atkinson[23-25] has conducted similar experiments on low-alloy steels in high-temperature aqueous environments under potentiostatic control. Atkinson's experiments were generally conducted at 288°-290°C in deoxygenated water (O_2 < 10 ppb) having a relatively low level of DH_2; H_2 <5% in the autoclave feedtank cover gas. Therefore, the level of DH_2 is estimated to be <0.8 cc H_2/kg H_2O (<70 ppb) for Atkinson's experiments. Atkinson showed[23] that the EAC that is induced in the steel by testing in a high-DO_2 environment could be duplicated by raising the potential of the steel in low-DO_2 low-DH_2 water to the same potential as was observed in the high-DO_2 testing; identical FCP rates were observed in both cases. Atkinson further suggested[24,25] that there was a synergism between the sulfur level of the steel and the potential to which the steel must be raised to induce EAC; i.e., the lower the steel sulfur content, the more noble the applied potential necessary to induce EAC. The present program was originally intended to expand Atkinson's observations to steels of both higher and lower sulfur contents. However, as will be discussed later in both Parts 1 and 2,

unexpected observations led to a more extensive study resulting in wider-ranging conclusions.

The crack growth results discussed herein will be presented in the "time-domain" format originally proposed by Shoji et al.[26,27] It is generally recognized that the correct mechanical crack-driving parameter in corrosion-FCP is related to the crack-tip strain rate ($\dot{\epsilon}_{ct}$), but unfortunately, there is no consensus definition of how to calculate $\dot{\epsilon}_{ct}$. Shoji proposed a parameter, the time-based air rate ($\dot{a}_b$), that is proportional to $\dot{\epsilon}_{ct}$. Although the exact relationship between $\dot{a}_b$ and $\dot{\epsilon}_{ct}$ is not defined, $\dot{a}_b$ can be used operationally in engineering assessments. $\dot{a}_b$ is defined as the mean FCP rate expected for a low-alloy steel in an air environment at a given level of ΔK and stress ratio ($R = K_{min}/K_{max}$), divided by the load rise-time for the fatigue cycle. The relationship of Eason et al.[28] is generally used to calculate the mean FCP rate for low-alloy steels in air. The time-based environmental rate ($\dot{a}_e$), is defined as the observed FCP rate (da/dN) divided by the load rise-time. In a time-domain plot, the mean air behavior is shown as a line of 1:1 slope ($\dot{a}_e = \dot{a}_b$), and EAC manifests itself by plotting well above the mean air line; i.e., $\dot{a}_e >> \dot{a}_b$.

Experiment 1 was conducted on low-sulfur Steel "A" in low-DO_2 low-DH_2water at 149°C. The steady-state corrosion potential under these conditions was about -0.518 V_{SHE}, but the experiment was started at an applied potential of -0.10 V_{SHE} (Test Phase 1 in Figure 1). Subsequent test phases were conducted at different levels of applied potential as shown in Figure 1. The results for Experiment 1 are plotted in Figure 2 using the time-domain format. Also shown, for comparison purposes, are results for Steels "A" and "D" tested under open-circuit conditions in high-DH_2 water at 149°C. At a temperature of 149°C, EAC manifests itself as a line parallel to the mean air line and approximately a factor of six above the air line.[19] Some hysterisis is observed in the transition from non-EAC to EAC behavior, depending upon whether the transition is approached from a condition of EAC or a condition of non-EAC. The hysterisis is related to the time delay for diffusional mass transport to remove sulfides from the crack tip, and is illustrated in Figure 2 by the results for Steel "D" in high-DH_2 water; (see also Ref. 19 for more discussion on the hysterisis). The results for Steel "A" in high-DH_2 water under open-circuit conditions show that EAC was not observed over a wide range of $\dot{a}_b$. However, the results for Experiment 1 in low-DH_2 water show that EAC was observed in Test Phases 1-3 at potentials over the range -0.277 V_{SHE} to -0.100 V_{SHE}. The potential was set at -0.660 V_{SHE} for Test Phase 4. Note in Figure 1 that in the early part of Test Phase 4 (called Phase 4a), the FCP rates remained at the EAC levels observed in Test

Phases 1-3; this may also be seen in Figure 2. However, the FCP rates then transitioned to non-EAC levels (Phase 4b), as may be seen in Figures 1 and 2. Delays in transitioning from EAC to non-EAC levels have been observed previously,[6,19,29] and are a result of the kinetics of mass transport in lowering crack-tip sulfide concentrations below the critical level. Subsequent increases in the applied potential in Test Phases 5-8 resulted in increases in FCP rates and the reestablishment of a state of EAC.

As stated earlier, under conditions of low-DO_2, very little potential gradient exists from the crack tip to the crack mouth. Crack tips are generally anoxic, and the crack-tip potential is generally active (electronegative) and relatively invariant regardless of the DO_2 level of the bulk water.[16,30] When the crack-mouth potential is significantly noble (electropositive) relative to that at the crack tip, the resulting potential gradient can drive sulfide ions toward the crack tip. This has been demonstrated by Andresen and Young[31] who, using crack-tip microsampling techniques, showed that sulfur levels at the crack tip were approximately an order of magnitude higher under high-DO_2 bulk water conditions than under high-DH_2 (low-DO_2) bulk water conditions. Andresen and Young observed EAC under the high-DO_2 bulk water conditions, but no EAC under the high-DH_2 (low-DO_2) conditions. These results, plus those of the present Experiment 1 and the earlier results of Atkinson,[23-25] demonstrate that raising the crack-mouth potential in low-DH_2 water, either potentiostatically or with oxygen additions to the bulk water, can induce a state of EAC. This is possible even with a low-sulfur steel like Steel "A".

Experiment 2 was conducted on medium-sulfur Steel "C" in low-DO_2 low-DH_2 water at 149°C. Test Phase 1 (see Figure 3) was conducted under open-circuit conditions at E_{corr} = -0.660 V_{SHE}, while Test Phase 2 was conducted with the specimen cathodically polarized to -0.800 V_{SHE}. As shown in Figure 4, EAC was not observed in either test phase. Test Phases 3-7 were conducted at increasingly noble potentials, and as may be seen in Figures 3 and 4, there was a marked increase in FCP rates at Test Phase 4 with a potential of -0.250 V_{SHE}. Approximately equivalent FCP rates (relative to the mean air line) were observed in Test Phases 4-7, suggesting that the effects of applied potential may saturate above a certain level. This saturation may be seen in Figure 5 by plotting the Environmental Ratio (ER = $\dot{a}_e/\dot{a}_b$) as a function of the potential. Note also that during Test Phase 8, the FCP rates tended to decrease toward the non-EAC level as the open-circuit potential transtitioned back toward E_{corr}. The behavior shown in Figure 5 is somewhat analogous to the effect of DO_2 upon E_{corr} as shown in Figure 6. Note that oxygen effects upon E_{corr} tend to saturate above a

certain level of DO_2. Plots like that of Figure 5 will not be shown for the other experiments to be discussed in this paper, but all of the results of these experiments produce curves that are qualitatively similar to Figure 5.

Experiment 3 was also conducted on medium-sulfur Steel "C" in low-DH_2 water at 149°C. The experiment was run under open-circuit conditions with DO_2 as a test parameter. The sequence of events is shown in Figure 7, and the results are plotted in Figure 8 using the time-domain format. Note that higher FCP rates were observed at the higher levels of DO_2, and the general correspondence between Figures 4 and 8, suggesting the equivalence of applied potential and DO_2 level in producing a given FCP response in low-DH_2 water. Potentials were measured during Experiment 3 and, in general, the ECP became more anodic with increasing levels of DO_2, not unlike Figure 6. These measurements, however, are not plotted because: 1) The DO_2 measurements were made with ChemMet ampoules which are not accurate at low levels, and 2) there is a time delay between the real-time ECP measurement and the DO_2 measurement of the autoclave effluent.

Experiment 4 was conducted on low-sulfur Steel "A" in low-DO_2 low-DH_2 water at 243°C. Test Phase 1 was conducted at the open-circuit potential of -0.516 V_{SHE}, and subsequent test phases were conducted at progressively more noble potentials (see Figure 9). The results, shown in Figure 10, show that above a potential of -0.300 V_{SHE}, FCP rates increase with increasing potential and reached the EAC curve by 0.00 V_{SHE} in Test Phase 6. The potentiostat was off during Test Phase 7, and FCP rates returned to the non-EAC level. EAC again resumed with the application of 0.00 V_{SHE} in Test Phase 8. FCP rates again trended toward the non-EAC line in Test Phase 11 when the potentiostat was again off.

Experiment 5 was conducted on medium-sulfur Steel "B" in low-DO_2 low-DH_2 water at 243°C. Test Phase 1 was conducted at the open-circuit potential of -0.624 V_{SHE}, and subsequent test phases were conducted at progressively more noble potentials (see Figure 11). As may be seen in Figure 11, the loading history of this experiment was complicated, with several changes in cyclic frequency occurring during the experiment. This was necessitated by the need to maintain a crack velocity ($V = \Delta a/\Delta time = 0.85\dot{a}_e$ for the waveform used in this study) high enough such that the crack tip intersects embedded sulfide inclusions in the steel at a rate high enough to initiate EAC; i.e., the rate of sulfide supply to the crack tip must be sufficiently high to provide the "critical" concentration. Wire and Li[11] have shown that for high-sulfur steels (like Steel "D"), the minimum crack velocity to initiate EAC is $V_{in} = 1.27 \times 10^{-6}/a$,

where "a" is the crack depth** in mm, and V is in mm/second. Medium-sulfur steels (like the present Steel "B") would require a higher critical crack velocity to initiate EAC because fewer sulfide inclusions are uncovered per unit of crack extension; hence, the crack extension per unit time must be higher. "a" was about 3 mm during Test Phase 4 of Experiment 5, and hence V_{in} should be at least $V_{in} = 1.27 \times 10^{-6}/3 = 4.23 \times 10^{-7}$ mm/second if the experiment had been conducted on a high-sulfur steel. Figure 12 shows that this was indeed about the velocity for Test Phases 3 and 4a, and significant EAC did not initiate. The non-initiation is not unexpected because of the lower sulfur content of Steel "B", and the velocity (cyclic frequency) was therefore increased part-way through Test Phase 4; i.e., Phase 4b. Significant EAC was still not observed, so both the potential and the cyclic frequency were increased for Test Phase 5, and EAC was indeed observed. The cyclic frequency was decreased during later test phases in order to continue to maximize the offset between the converging EAC and non-EAC curves in this regime. Nevertheless, EAC was induced in this medium-sulfur steel, and it is speculated that the critical potential might have been about -0.150 V_{SHE} had higher frequencies been employed in Test Phase 4. The final phase was conducted under high-DH_2 conditions and as will be noted in Figure 12, the FCP rates rapidly approached the mean non-EAC line as the open-circuit potential became more active (Figure 11).

Experiment 6 was conducted on high-sulfur Steel "D" in low-DO_2 low-DH_2 water at 243°C. Test Phase 1 was conducted at the open-circuit potential of -0.565 V_{SHE} (see Figure 13). As shown in Figure 14, EAC was observed under open-circuit conditions in Test Phase 1, and this is in agreement with previous studies on this heat,[14,15,19] all of which exhibited EAC under open-circuit conditions in quiescent water at 243°F. Atkinson[24,25] had shown that he could turn off a case of EAC in a 0.015%-sulfur steel by polarizing the specimen to more active (electronegative) potentials. Therefore, subsequent phases of Experiment 6 utilized progressively more active potentials in an attempt to turn EAC off. Figure 14 shows that it was not possible to suppress EAC, even at potentials of -1.600 V_{SHE}, a potential that is beyond the stability point of water. The inability to suppress EAC at large cathodic underpotentials was unexpected in light of Atkinson's observations on a steel of somewhat lower sulfur content.

** "a" is the mass-transport path and hence would be measured from the notch in a CT specimen.

Experiment 7 was conducted on low-sulfur Steel "A" under low-DO_2 high-DH_2 conditions at 149°C. Test Phase 1 was conducted at the open-circuit potential of E_{corr} = -0.666 V_{SHE}, and Test Phase 2 was conducted at an applied potential of -0.250 V_{SHE} (see Figure 15). The results are plotted in Figure 16 and as will be noted, EAC was not observed in either test phase. Also plotted, for comparison purposes, are results for an experiment on the same heat of steel under open-circuit conditions in high-DH_2 water at 149°C, and these results show that EAC would not be expected under open-circuit conditions over a wide range of a_b.

Experiment 8 was conducted on low-sulfur Steel "A" under low-DO_2 high-DH_2 conditions at 243°C. Test Phase 1 was conducted at the open-circuit potential of E_{corr} = -0.744 V_{SHE}, and subsequent test phases were conducted at progressively more noble potentials (see Figure 17). The cyclic frequency was reduced at Test Phase 8 in order to restore the maximum offset between the EAC and non-EAC curves in this regime. As will be seen in Figure 18, EAC was not observed at any potential up to +0.200 V_{SHE}. From Figure 6 it will be seen that +0.200 V_{SHE} is about the most noble potential that a steel could be raised to by high levels of DO_2, and higher potentials were therefore not imposed. The inability to induce EAC at rather high potentials in high-DH_2 water is in agreement with the result for Experiment 7, although the latter experiment went only to -0.250 V_{SHE}. This result, however, would not have been expected based on Atkinson's results[24] in low-DO_2 low-DH_2 water at 288°C; Atkinson was able to induce EAC in a steel containing 0.005% sulfur at an applied potential of 0.00 V_{SHE}. The differences between the observations in the present Experiments 7 and 8, and Atkinson's observations will be discussed more fully in Part 2 of this paper.[17]

Finally, Experiment 9 was conducted on high-sulfur Steel "D" in low-DO_2 high-DH_2 water at 243°C. The first test phase was conducted at the open circuit potential E_{corr} = -0.694 V_{SHE}, and subsequent test phases were conducted at progressively more active potentials (see Figure 19). As will be seen in Figure 20, EAC was observed in all test phases, even down to an applied potential of -1.125 V_{SHE}. Again, this result was unexpected based on the earlier observations of Atkinson,[24,25] where EAC was suppressed in a 0.015% sulfur steel tested in low-DO_2 low-DH_2 water at 290°C by the application of cathodic underpotentials. The differences between the present observation and those of Atkinson will be addressed in Part 2 of this paper.[17]

SUMMARY

Nine FCP experiments were conducted on low-alloy steels of varying sulfur content in an elevated temperature environment; eight experiments were conducted under potentiostatic control, and one under open-circuit conditions. The level of dissolved hydrogen (DH_2) was a parameter in these experiments, and two levels were utilized: low-DH_2 = < 1 cc H_2/kg H_2O, and high-DH_2 = 30-55 cc H_2/kg H_2O.

EAC could be induced in low- and medium-sulfur steels (S=0.002, 0.010, and 0.011%) when tested in low-DO_2 low-DH_2 water at temperatures of 149°C and 243°C by anodically polarizing the specimens. None of these steels exhibited EAC under open-circuit conditions. The level of anodic overpotential was dependent upon the sulfur content of the steel, and increased as sulfur content decreased. These observations are in agreement with those of Atkinson.[23-25] On the other hand EAC could not be suppressed in low-DO_2 low-DH_2 water by application of cathodic underpotentials in a high-sulfur steel (0.026% S) that normally exhibits EAC under open-circuit conditions in quiescent water. EAC persisted, even at very large cathodic underpotentials (-1.60 V_{SHE}), and this is at variance with the observation of Atkinson who was able to suppress EAC in a 0.015% steel by cathodic polarization in low-DO_2 low-DH_2 water.

An experiment was conducted on a medium-sulfur (S = 0.010%) steel in low-DH_2 water at 149°C employing DO_2 as a test parameter. Elevated levels of DO_2 (> 50 ppb DO_2) accelerated FCP rates relative to those at lower levels of DO_2. The FCP response to DO_2 level was quite similar to that due to applied potential: both high levels of DO_2 and anodic polarization produced higher FCP rates in low-DH_2 water, while low levels of DO_2 and/or cathodic potentials produced lower FCP rates. These observations are in agreement with those of Atkinson.[23]

EAC could not be induced in the low-sulfur steel (S = 0.002%) when testing in low-DO_2 high-DH_2 water at temperatures of 149°C and 243°C by polarizing the specimens to -0.250 V_{SHE} and +0.200 V_{SHE}, respectively. On the other hand, EAC could not be suppressed in the high-sulfur (0.026% S) tested in low-DO_2 high-DH_2 water at 243°C despite polarizing to a potential of -1.125 V_{SHE}.

Several of the above results were not expected, and the reasons for these observations will be discussed in Part 2[17].

ACKNOWLEDGEMENTS

This work was performed under a U.S. Department of Energy contract with the Bettis Atomic Power Laboratory, a unit of Westinghouse Electric Corporation. The efforts of S. A. Derry, technician, in helping make the experiments a success are greatly appreciated, as are the helpful suggestions of a colleague, Dr. J. P. Moran.

REFERENCES

1. T. Kondo, T. Kikuyama, H. Nakajima, M. Shindo, and R. Nagasaki, *Corrosion Fatigue: Chemistry, Mechanics, and Microstructure, NACE-2, p. 539 (1972)*

2. T. Kondo, T. Kikuyama, H. Nakajima, and M. Shindo, Mechanical Behavior of Materials, Proc. Int. Conf. Mech. Behavior of Matls., Vol. 3, Society of Matls. Sci. Japan, p. 319 (1972)

3. D.R. Tice, *Corrosion Science* **25**, 705 (1985)

4. J.H. Bulloch, *Res Mechanica* **26**, 95 (1989)

5. L.A. James, *Welding Research Council Bulletin 404*, p. 1 (1995)

6. W.A. VanDerSluys and R.H. Emanuelson, EPRI TR-102796, Vol. 1 & 2 (1993)

7. G. Wranglén, *Corrosion Science* **14**, 331 (1974)

8. S. Matsushima, Y. Katada, S. Sato, and N. Nagata, *Corrosion Control, 7th APCCC*, Vol. 1, Int. Academic Publishers, Beijing, p. 112 (1991)

9. A. Turnbull and J.G.N. Thomas, *J. Electrochemical Society* **129**, 1412 (1982)

10. A. Turnbull and M. Psaila-Dombrowski, *Corrosion Science* **33**, 1925 (1992)

11. G.L. Wire and Y.Y. Li, *Fatigue and Fracture-1996-Volume 1*, ASME Publication PVP-Vol. 323, p. 269 (1996)

12. A. Turnbull, *Corrosion-Fatigue: Mechanics, Metallurgy, Electrochemistry and Engineering*, ASTM STP 801, p. 351 (1983)

13. W.H. Hartt, J.S. Tennant, and W.C. Hooper, *Corrosion-Fatigue Technology*, ASTM STP 642, p. 5 (1978)

14. L.A. James, G.L. Wire, and W.H. Cullen, *J. Pressure Vessel Technology* **117**, 238 (1995)

15. L.A. James, H.B. Lee, and G.L. Wire, *ibid.* **119**, in press (1997)

16. G. Gabetta and E. Caretta, *Corrosion Chemistry Within Pits, Crevices, and Cracks*, Her Majesty's Stationery Office, London, p. 287 (1987)

17. W.C. Moshier and L.A. James, *Corrosion Science*, this issue

18. R.J. Stofanak, T.J. Poskie, Y.Y. Li, and G.L. Wire, *Proc. Sixth Int. Symp. Environmental Degratation of Matls. in Nuclear Power Systems - Water Reactors*, TMS-AIME, p. 757 (1993)

19. L.A. James, *J. Pressure Vessel Technology* **116**, 122 (1994)

20. L.A. James, *ibid.* **117**, 341 (1995)

21. A. Saxena and S.J. Hudak, *Int. J. Fracture* **14**, 453 (1978)

22. D.D. Macdonald, A.C. Scott, and P. Wentrcek, *J. Electrochemical Society* **126**, 1618 (1979)

23. J.D. Atkinson, *Proc. Fourth Int. Symp. Environmental Degradation of Matls. in Nuclear Power Systems - Water Reactors*, NACE, p. 8.64 (1990)

24. J.D. Atkinson, cited in J.H. Bulloch, *Int. J. Pressure Vessels & Piping* **53**, 1 (1993)

25. J.D. Atkinson, J. Yu, and Z.-Y. Chen, *Corrosion Science* **38**, 755 (1996)

26. T. Shoji, H. Takahashi, M. Suzuki, and T. Kondo, *J. Engng. Matls. & Technol.* **103**, 298 (1981)

27. T. Shoji, H. Takahashi, H. Nakajima, and T. Kondo, NUREG/CP-0044, Vol. 2, p. 143 (1983)

28. E.D. Eason, S.P. Andrew, S.B. Warmbrodt, E.E. Nelson, and J.D. Gilman, *Nuclear Engng. & Design* **115**, 23 (1989)

29. P. Combrade, M. Foucault, and G. Slama, *Proc. Third Int. Symp. Environmental Degradation of Matls. in Nuclear Power Systems - Water Reactors*, TMS-AIME, p. 269 (1988)

30. G. Gabetta, M.M. Radaelli, and M. Ferrari, NUREG/CP-0112, Vol. 2, p. 129 (1990)

31. P.L. Andresen and L.M. Young, *Corrosion* **51**, 223 (1995)

32. J.D. Atkinson, S.T. Cole, and J.E. Forrest, NUREG/CP-0044, Vol. 2, p. 173 (1983)

33. M.E. Indig, J.E. Weber, and D. Weinstein, *Reviews on Coatings & Corrosion* **5**, 173 (1982)

34. Y. Katada, N. Nagata, and S. Sato, *ISIJ Int. J.* **33**, 877 (1993)

TABLE 1

COMPOSITION OF THE STEELS

Designator	Alloy	Heat No	C	Mn	P	S	Si	Mo	Cu	Ni	Cr
"A"	Superclean	A9214	0.24	0.04	0.004	0.002	0.02	0.51	0.05	3.75	1.93
"B"	A508-2	124H448	0.24	0.68	0.011	0.011	0.20	0.63	0.07	0.74	0.34
"C"	A508-4*	122Z195	0.18	0.29	0.010	0.010	0.19	0.50	0.08	3.37	1.75
"D"	A302-B*	21478-10	0.20	1.25	0.021	0.026	0.22	0.51	0.22	0.22	0.14

* Average of multiple measurements

TABLE II

ROOM TEMPERATURE MECHANICAL PROPERTIES

Designator	Alloy	Heat No.	0.2% Offset Yield (MPa)	Ultimate Strength (MPa)	Percent Elongation	Percent Red. Area
"A"	Superclean*	A9214	607.7	732.2	26.8	79.1
"B"	A508-2*	124G448	444.0	598.5	24.5	69.8
"C"	A508-4*	122Z195	654.2	767.4	22.7	71.6
"D"	A302-B	21478-10	406.8	544.7	-	-

* Average of multiple measurements.

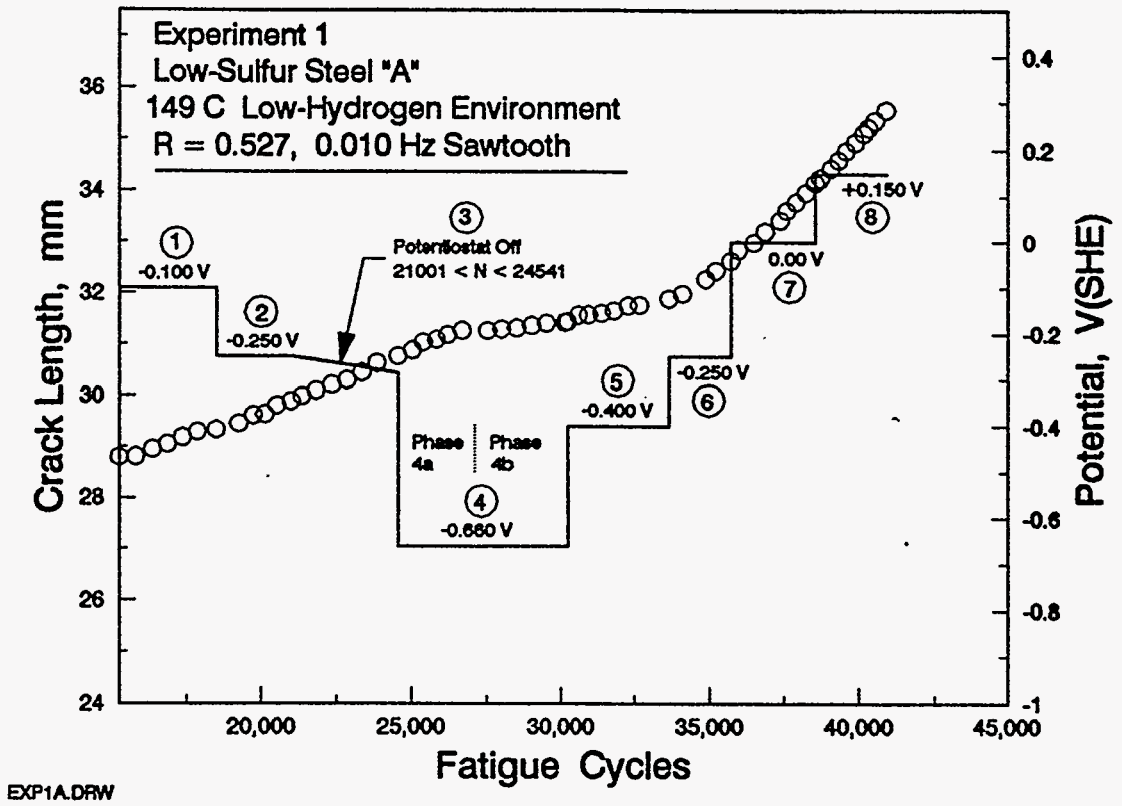

Figure 1: Crack length and applied potential plotted as a function of fatigue cycles for Experiment 1.

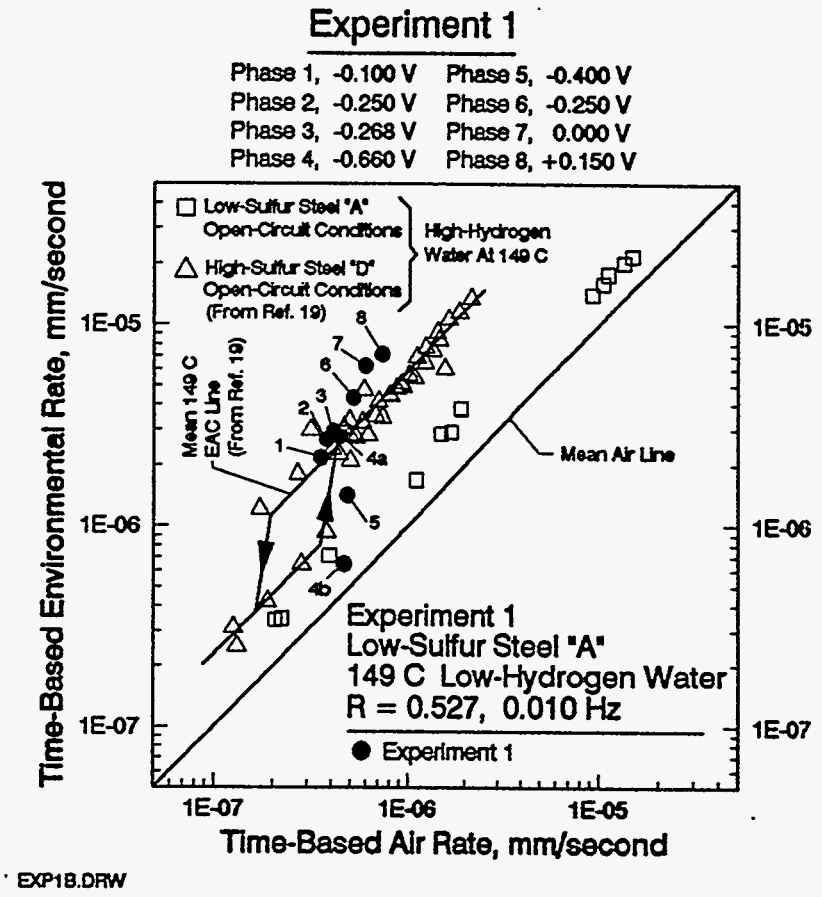

Figure 2: Time-domain plot of the results for Experiment 1.

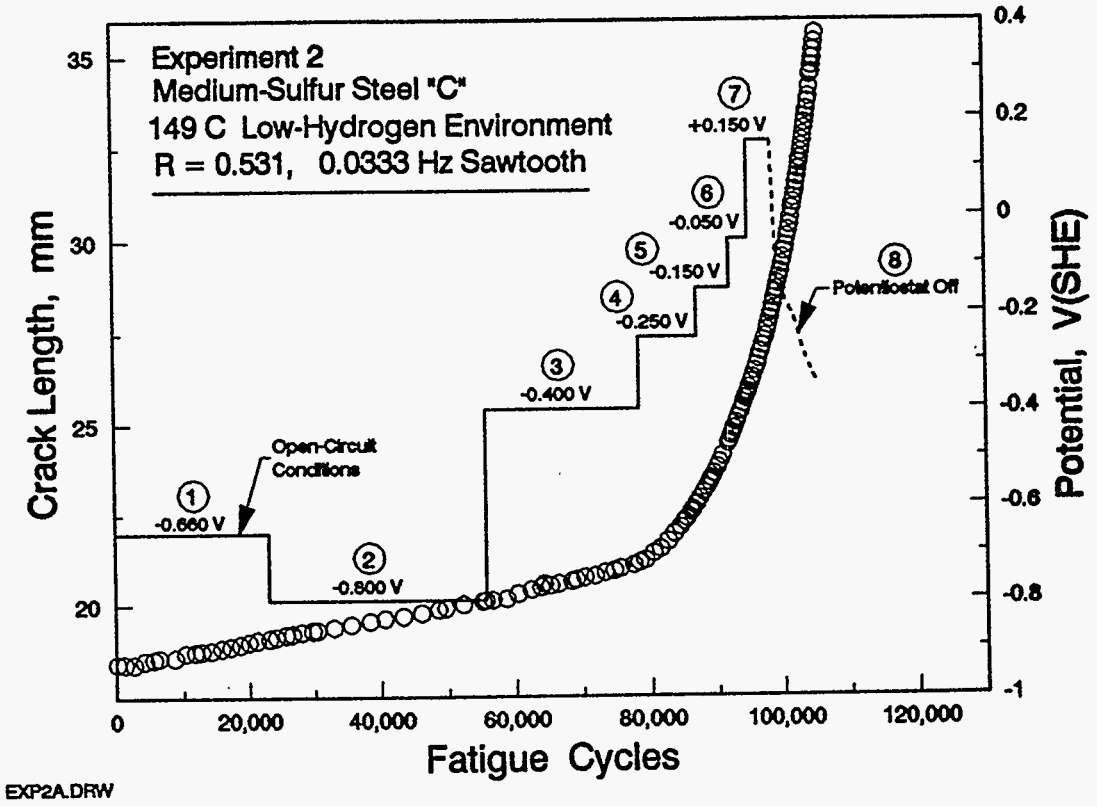

Figure 3: Crack length and applied potential plotted as a function of fatigue cycles for Experiment 2.

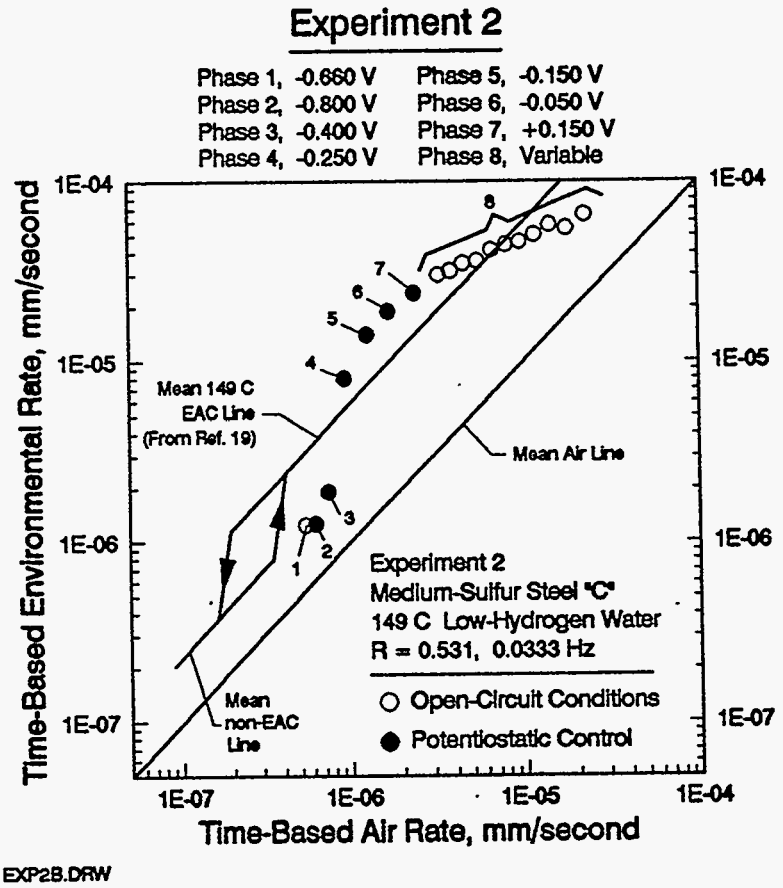

Figure 4: Time-domain plot of the results for Experiment 2.

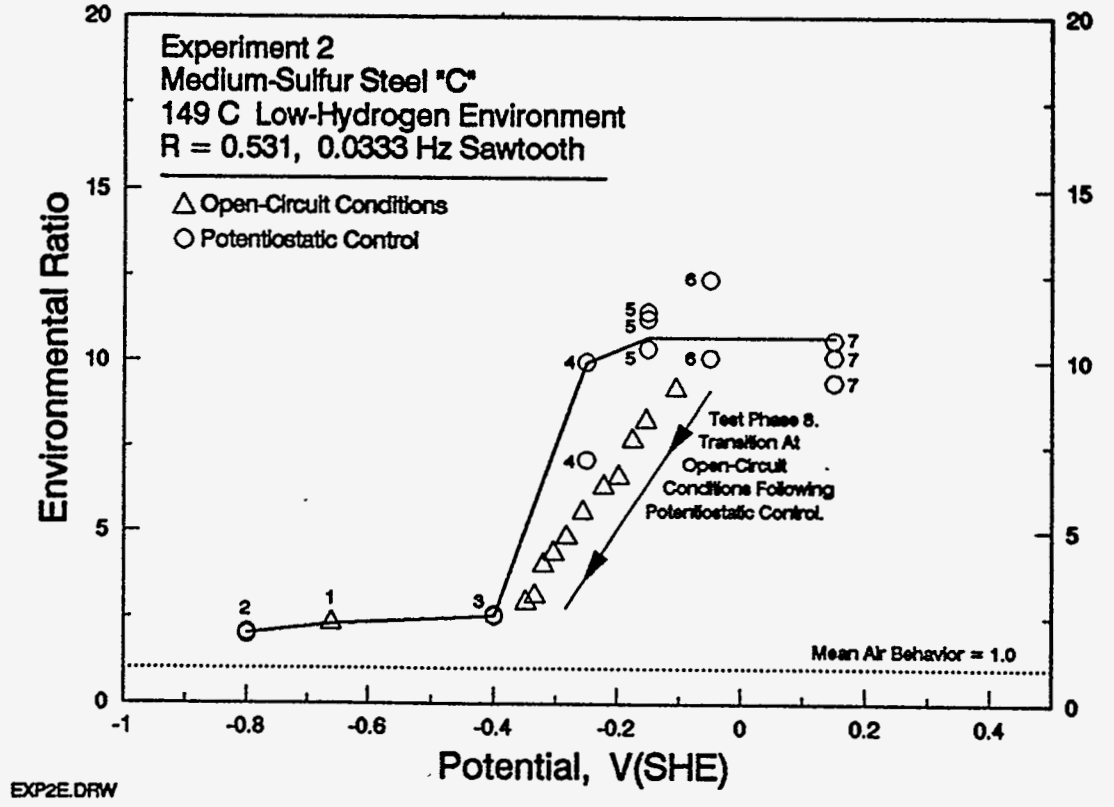

Figure 5: Environmental Ratios observed in Experiment 2 as a function of the potential

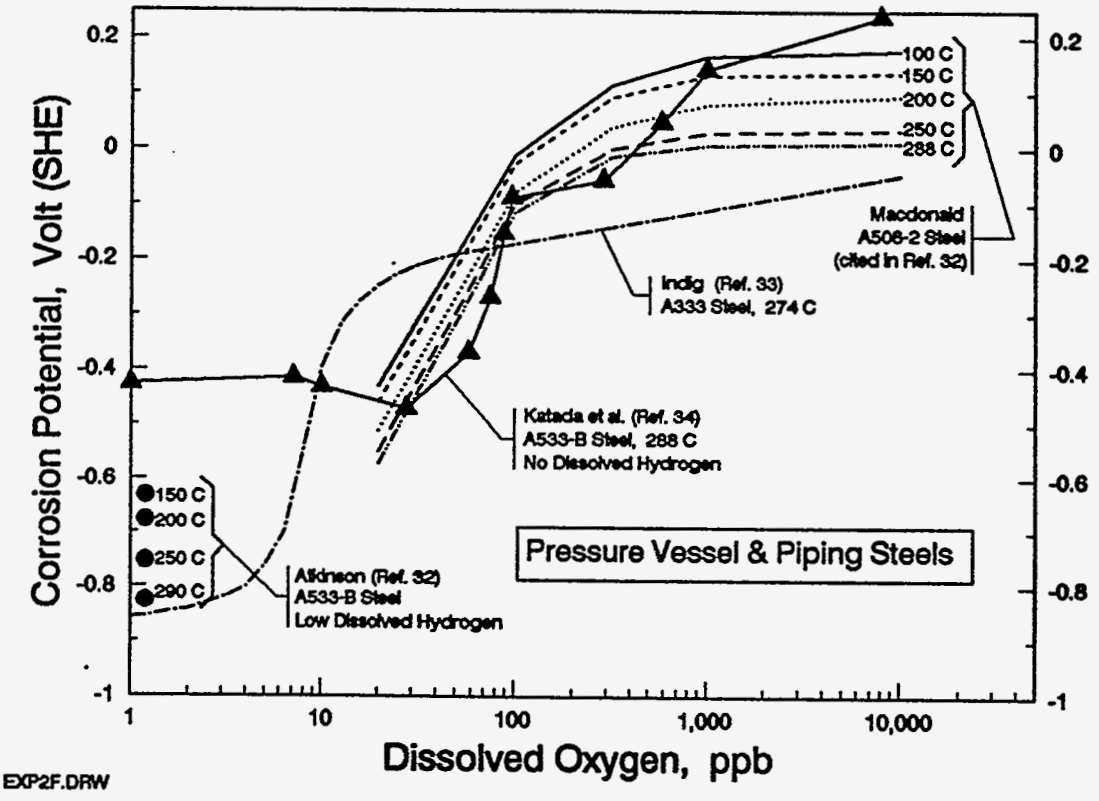

Figure 6: Corrosion potential for several low-alloy and carbon steels as a function of dissolved oxygen.

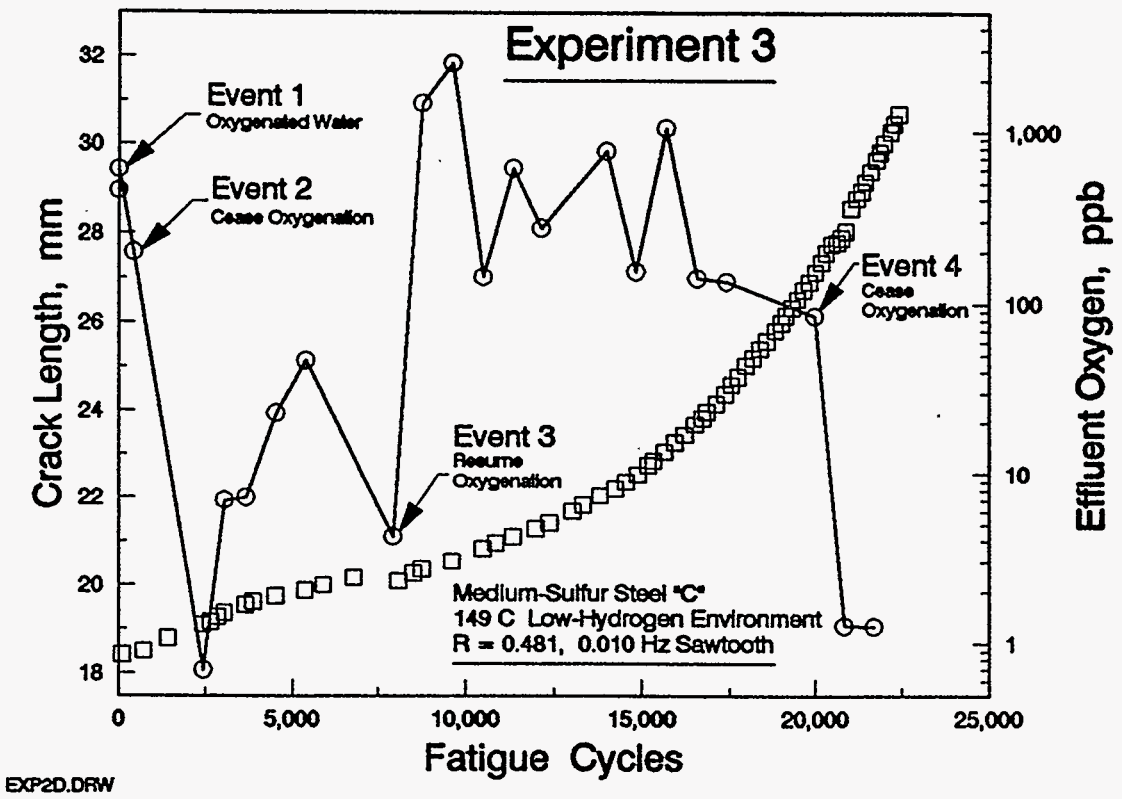

Figure 7: Crack length and autoclave effluent oxygen level plotted as a function of fatigue cycles for Experiment 3.

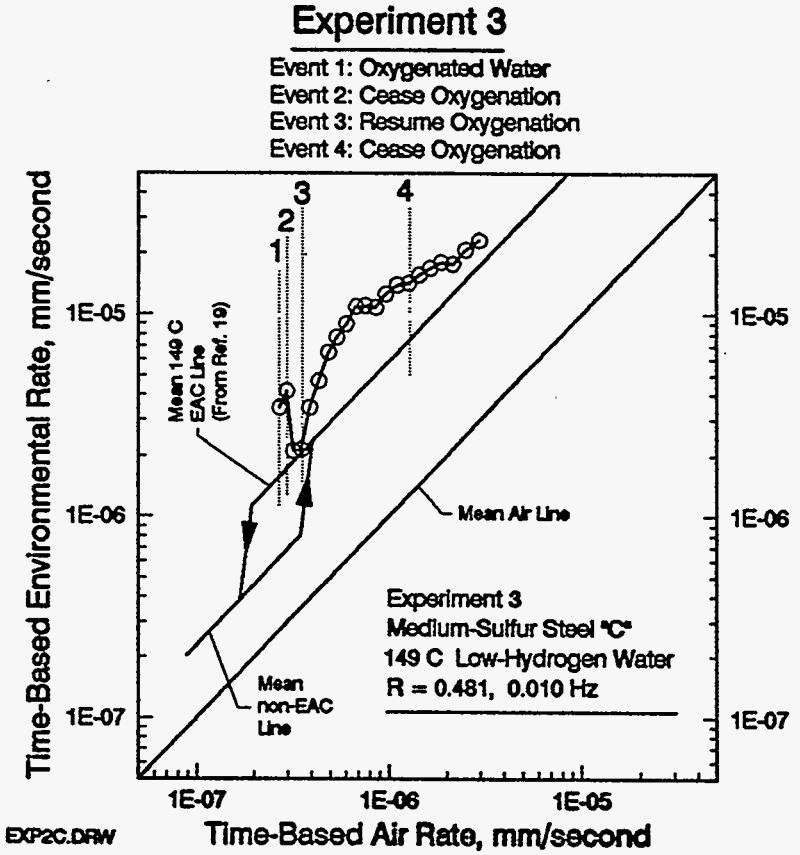

Figure 8: Time-domain plot of the results for Experiment 3. Compare with the results for Experiment 2 in Figure 4.

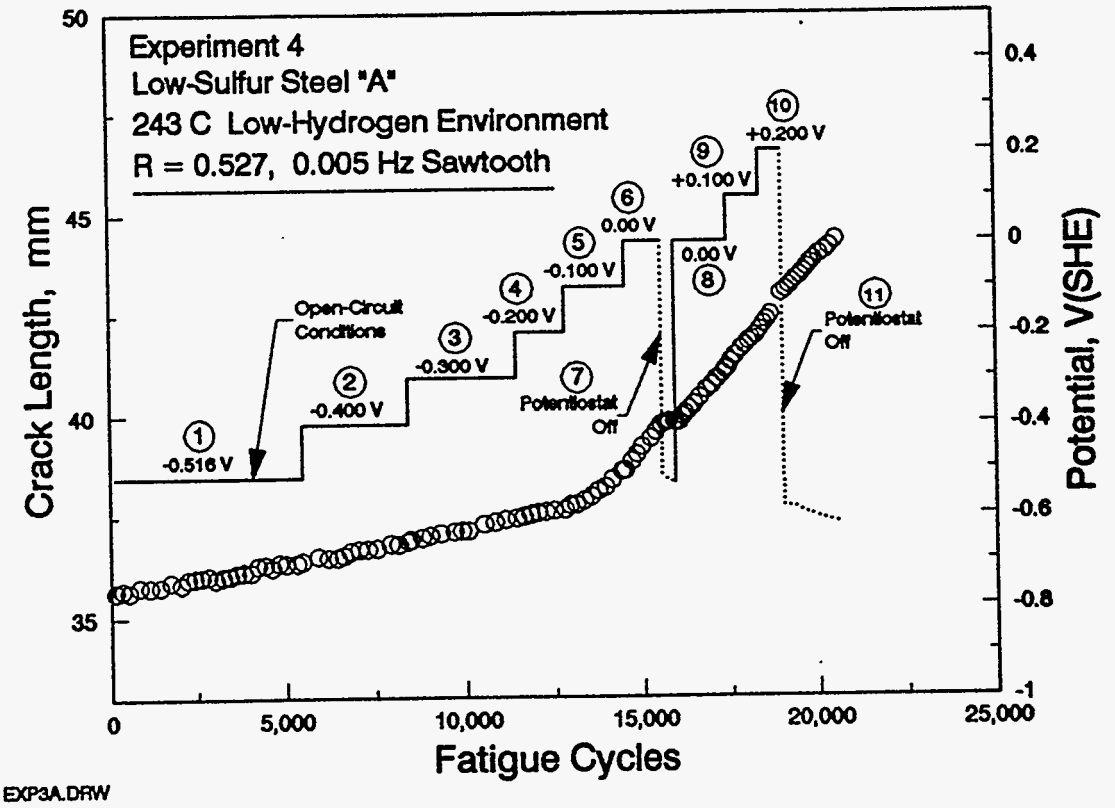

Figure 9: Crack length and applied potential plotted as a function of fatigue cycles for Experiment 4.

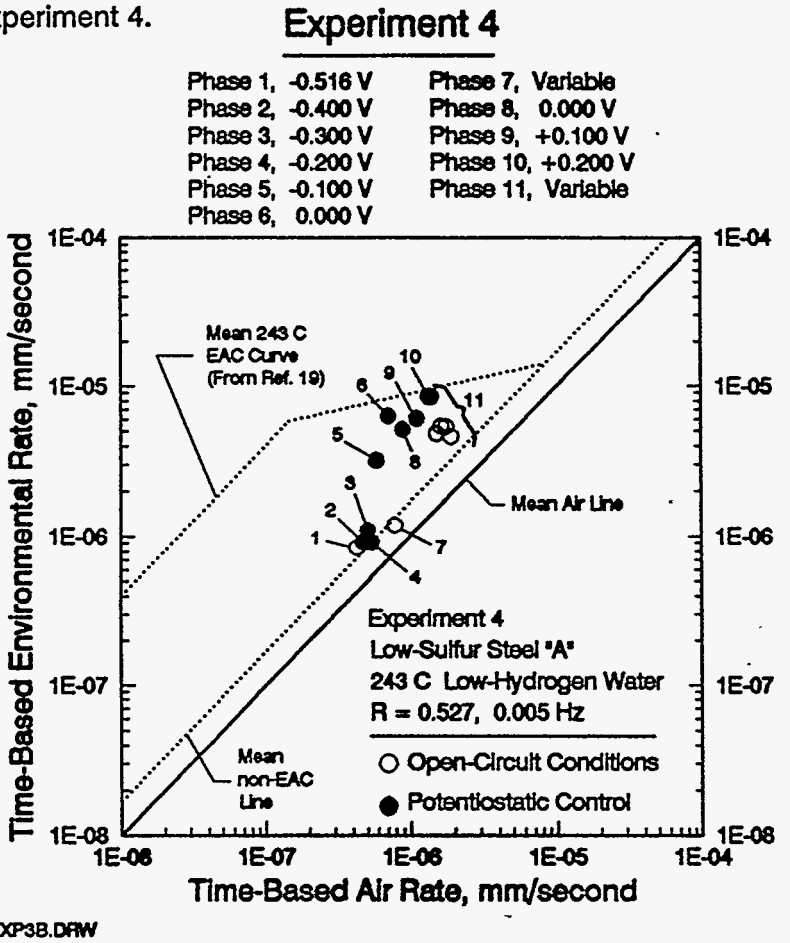

Figure 10: Time-domain plot of the results for Experiment 4.

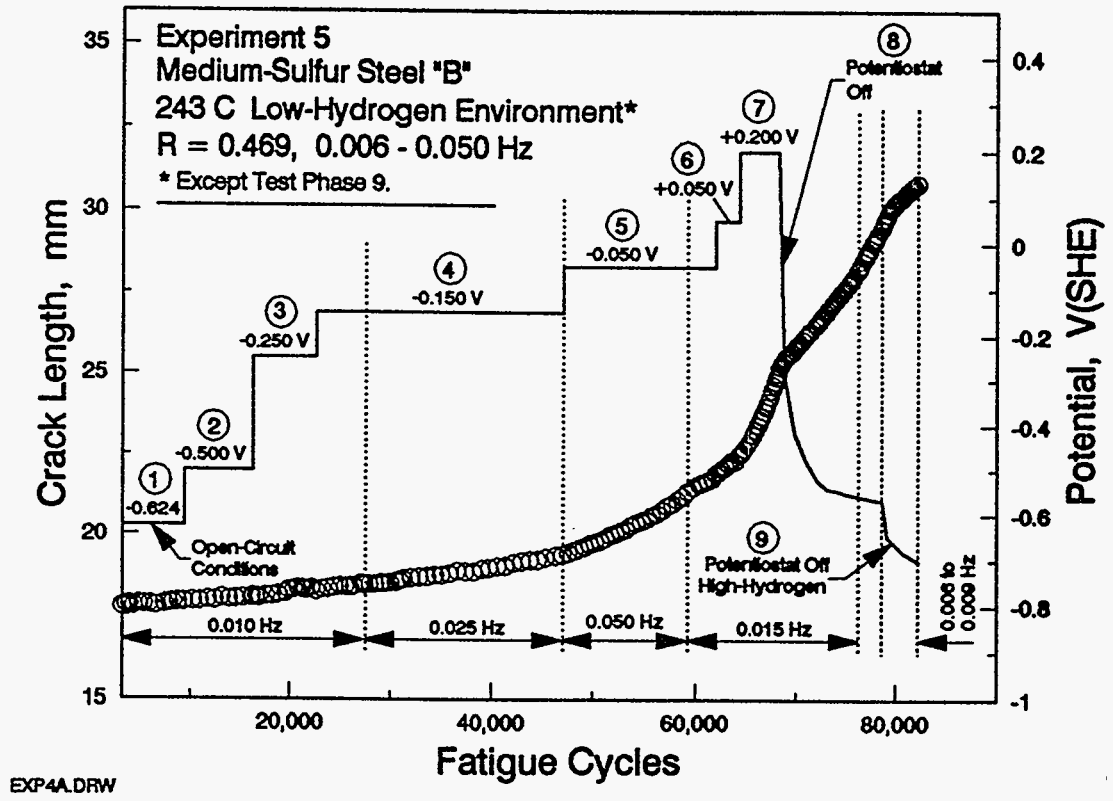

Figure 11: Crack length and applied potential plotted as a function of fatigue cycles for Experiment 5.

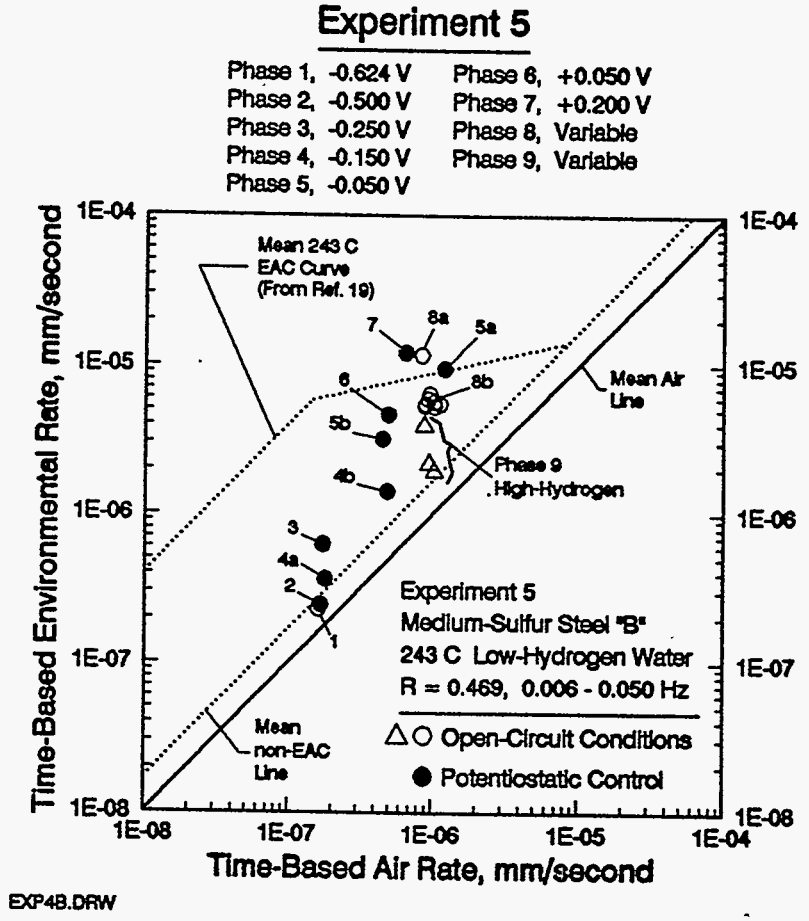

Figure 12: Time-domain plot of the results for Experiment 5.

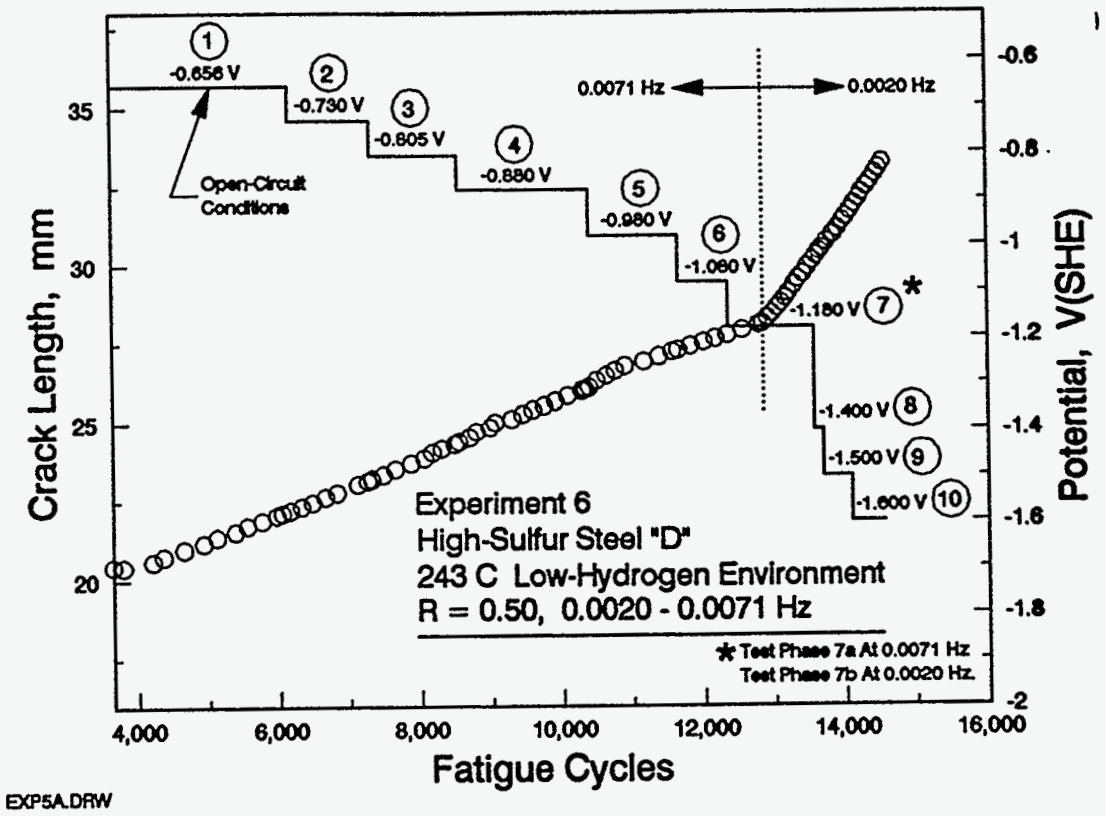

Figure 13: Crack length and applied potential plotted as a function of fatigue cycles for Experiment 6.

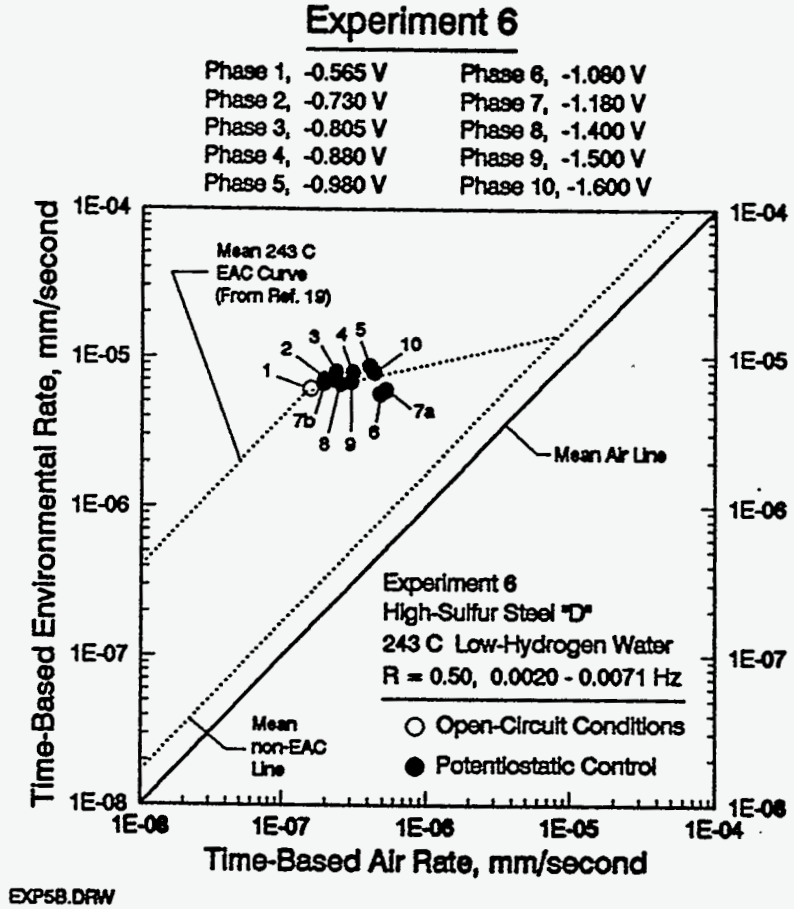

Figure 14: Time-domain plot of the results for Experiment 6.

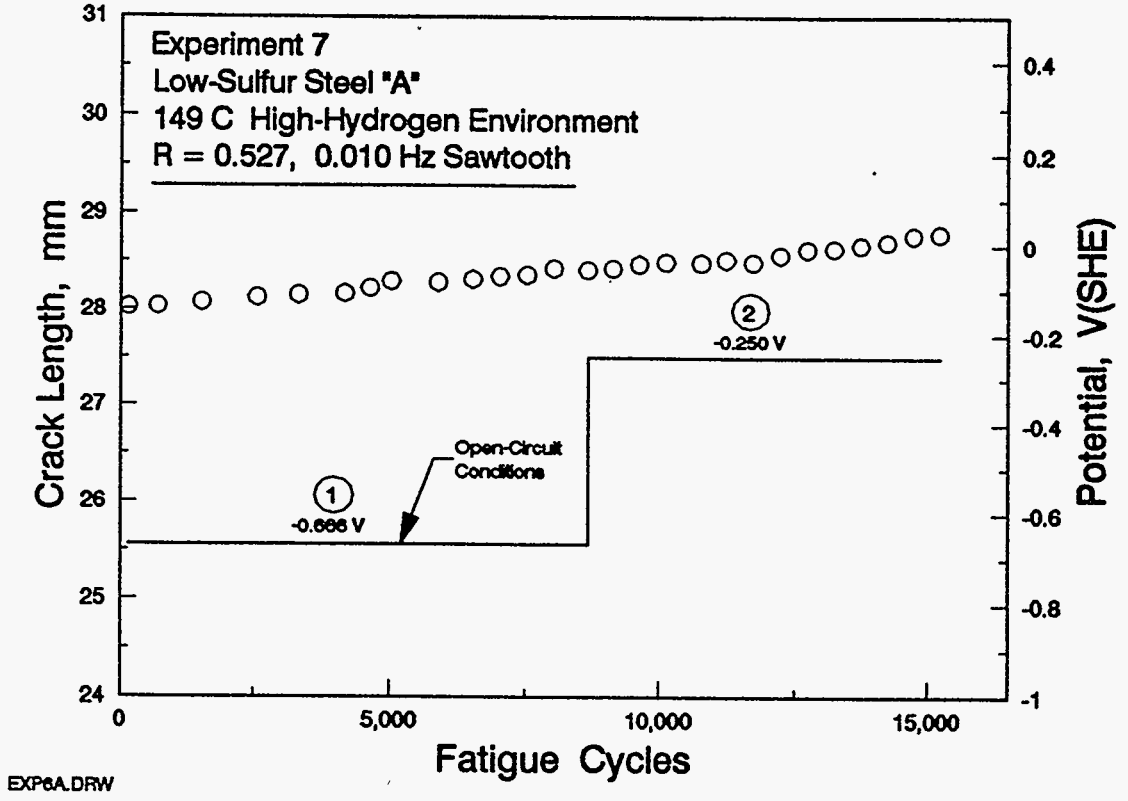

Figure 15: Crack length and applied potential plotted as a function of fatigue cycles for Experiment 7.

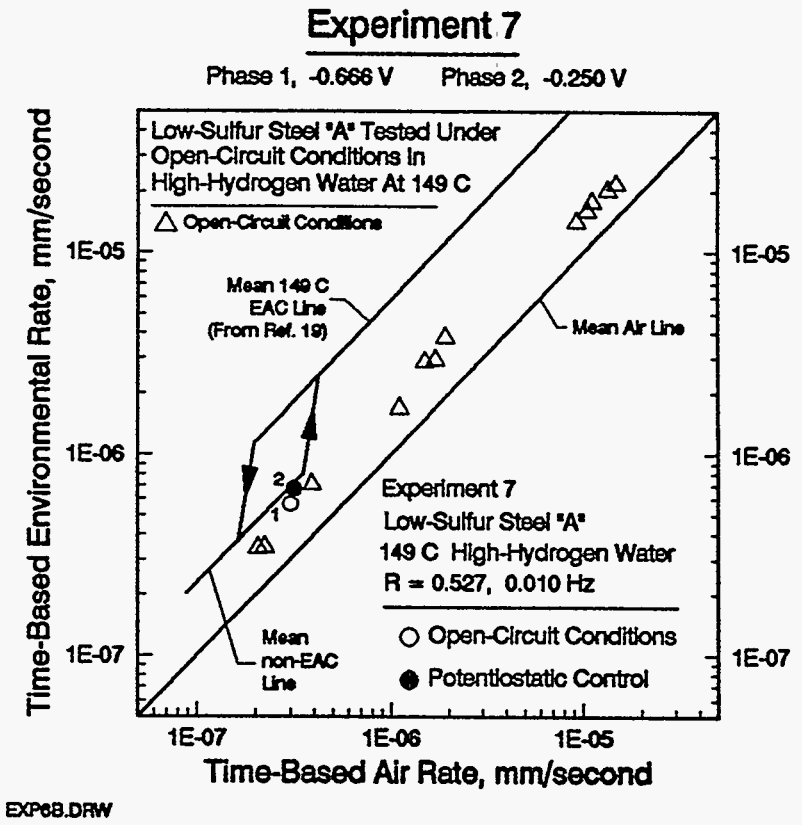

Figure 16: Time-domain plot of the results for Experiment 7.

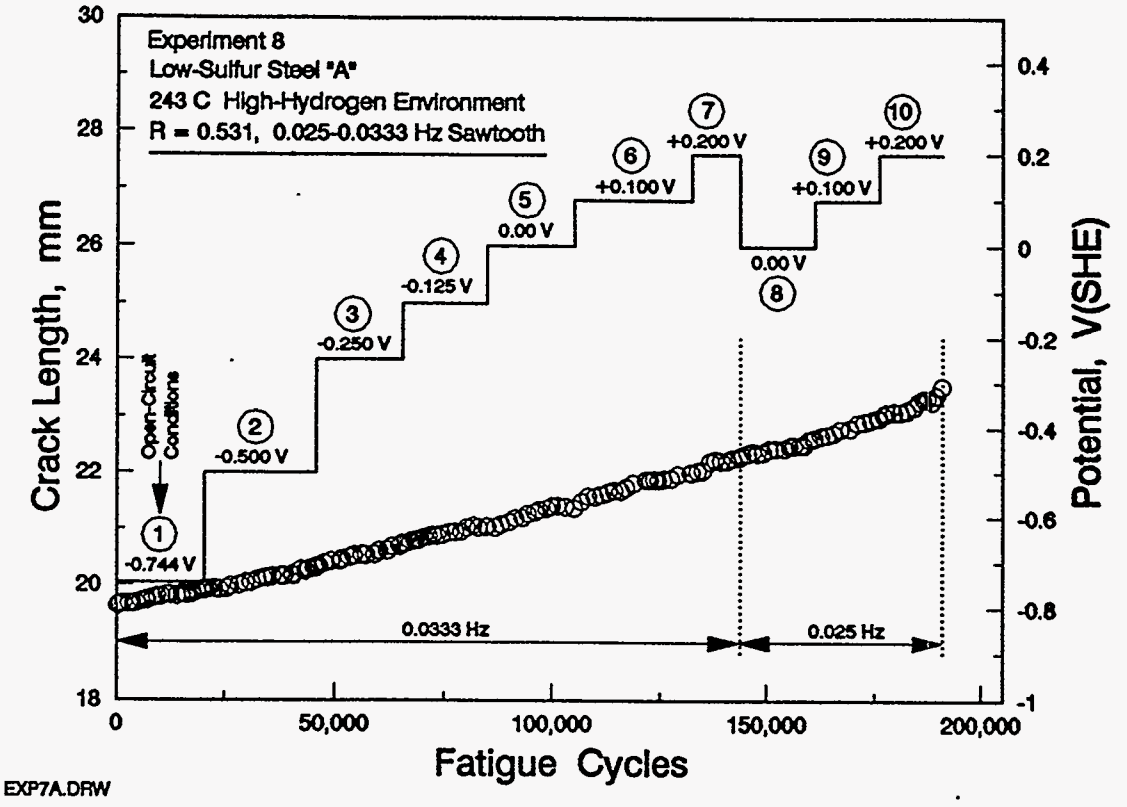

Figure 17 Crack length and applied potential plotted as a function of fatigue cycles for Experiment 8.

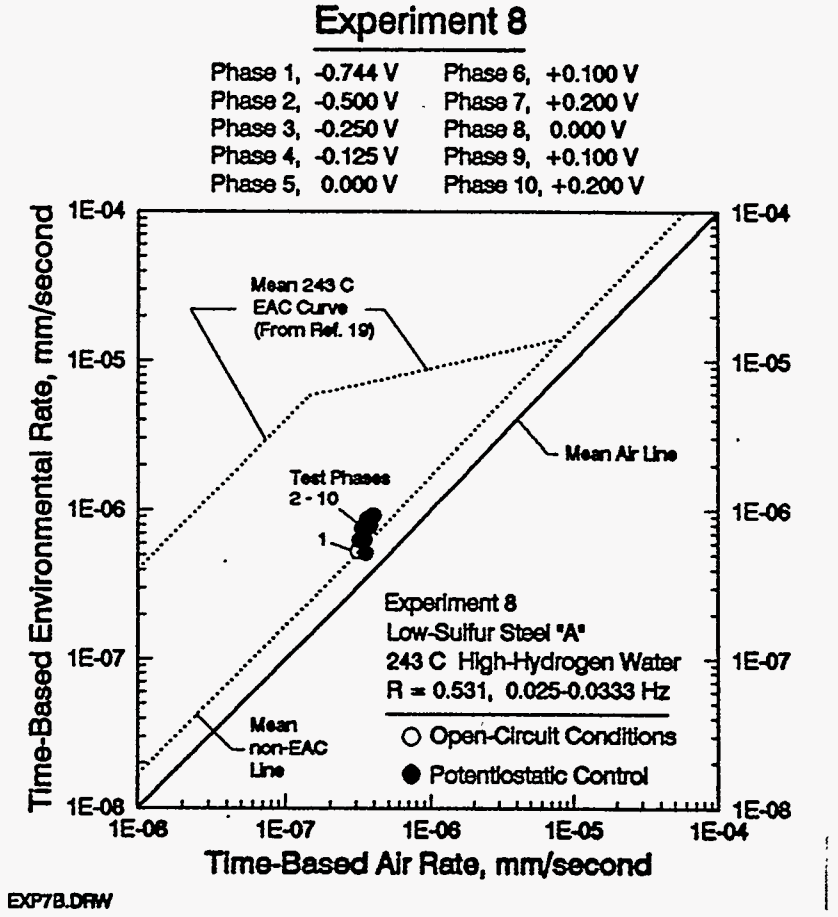

Figure 18 Time-domain plot of the results for Experiment 8.

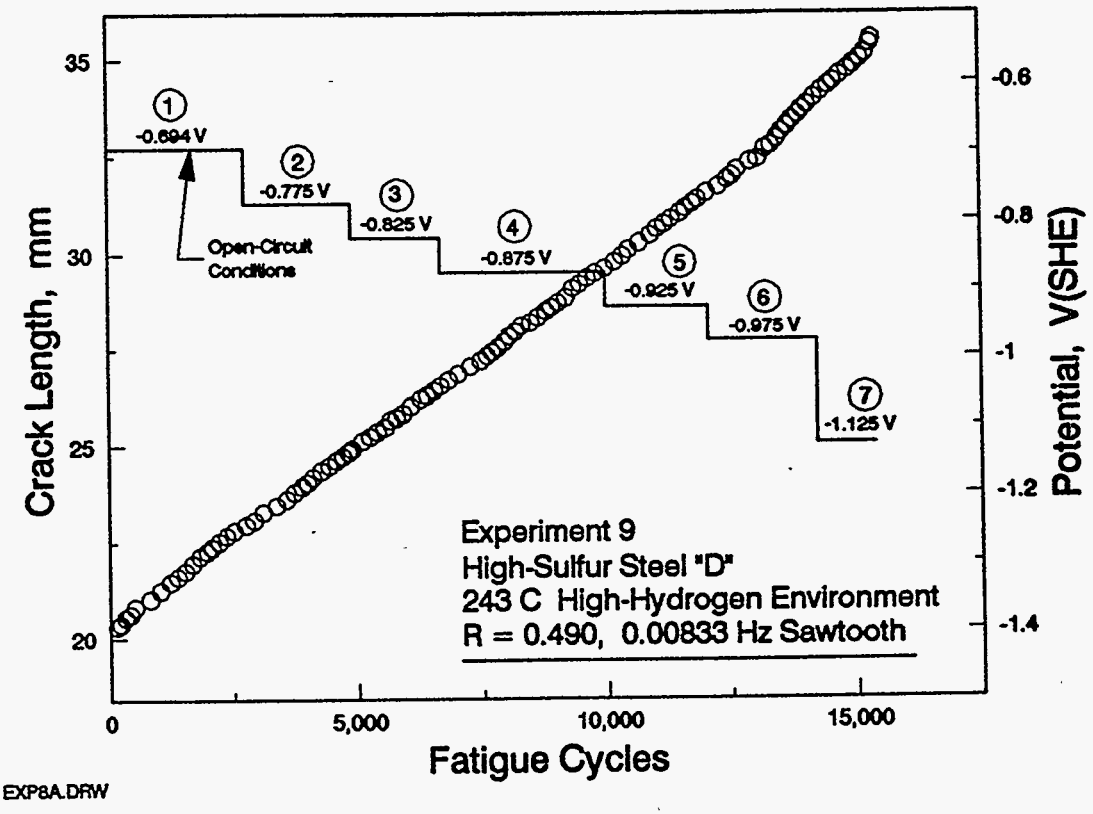

Figure 19 Crack length and applied potential plotted as a function of fatigue cycles for Experiment 9.

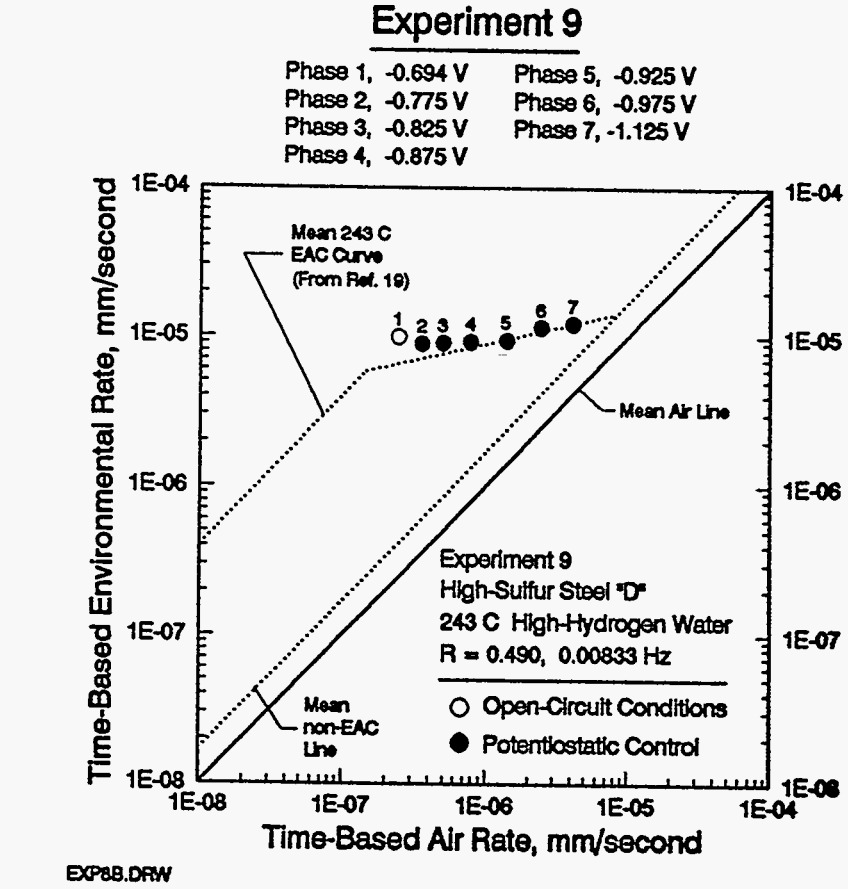

Figure 20 Time-domain plot of the results for Experiment 9.